Numerical study on explosion characteristics of wind turbine blade under lightning induced arc

Wanshui Yu
State Key Lab of Alternate Electrical Power System with Renewable Energy Sources
North China Electric Power University
Beijing, China
yws@ncepu.edu.cn

Qingmin Li
State Key Lab of Alternate Electrical Power System with Renewable Energy Sources
North China Electric Power University
Beijing, China
lqmeee@ncepu.edu.cn

Zixin Guo
China Electric Power Research Institute
Beijing, China
guozixin@epri.sgcc.com.cn

Hanwen Ren
State Key Lab of Alternate Electrical Power System with Renewable Energy Sources
North China Electric Power University
Beijing, China
rhw112118@163.com

Wah Hoon Siew
Department of Electronic & Electrical Engineering
University of Strathclyde
Glasgow, United Kingdom
wh.siew@strath.ac.uk

***Abstract*—For enhancing the lightning protection abilities of wind turbine blades, there is the need to study the mechanical explosion characteristics when the blades suffer from lightning induced arc intrusion. In this paper, a magnetohydrodynamic (MHD) model of lightning induced arc intrusion into the blade was developed, and the airflow and gas pressure distribution were calculated accordingly. The simulation results show that the huge pressure generated at the trailing edge of the blade should be the main cause of the trailing edge cracking. The research presented in this paper provides a theoretical basis for improving the structural design of the blade from the lightning protection perspective.**

Keywords—wind turbine blade, lightning induced arc, blade explosion process, MHD, air pressure distribution

I. INTRODUCTION

Lightning strikes on wind turbines are also becoming an increasingly prominent problem. More than 3/5 of natural accidents on turbines are caused by lightning strikes, which is a serious threat to the normal operation of wind farms. According to the lightning event statistics of 508 wind turbines in US wind farms, 304 blades were struck by lightning in 5 years. Thus, on average, each wind turbine has one blade damage due to lightning every 8.4 years [1].

To improve the lightning protection of the wind turbine blades, it is recommended to install discrete lightning receptors and down conductors on the blades as lightning protection system [2]. However, the lightning protection system may fail to intercept the lightning downward leader. When the interception misses, the lightning can easily penetrate the blade surface, which will result in the lightning arc into the blade chamber. The coupled effects of heat, magnetic and airflow caused by the lightning arc may tear or break the blade, or even burn it, as shown in Fig. 1.

(a) Edge crack (b) Complete cracking of blade

Fig. 1 Blade damage by the invasion of lightning induced arc

On the one hand, many studies have contributed to improving the lightning protection system of wind turbine blades [3]–[6]. On the other hand, the damage to blades by lightning strike can be reduced by strong mechanical structure design, which requires the study of mechanical explosion characteristics of blades under lightning induced arcs. The damage characteristics of blade materials under impulse current and the tolerance of different blade materials were studied by both simulation and experiment [7]–[9]. Nevertheless, structural damage characteristics of blade materials remain under preliminary exploration. By testing the pressure distribution inside the enclosed cavity under the effect of impulse current, the effect of different water vapor concentration inside the blade on the damages was investigated [10]. However, physical characteristics of mechanical damage to wind turbine blades under lightning-induced arcs have not been explored in depth. Additional discovery of the intrinsic characteristics of mechanical explosions remains to be carried out.

Under the effect of lightning induced arcs, the multi fields of internal environment of the blade chamber are coupled. In order to study the explosion characteristics of the blade, the distribution of temperature, airflow and electromagnetic inside the blade needs to be studied.

In this paper, a MHD model of the arc inside the blade was established considering the typical path of lightning induced arc. The distributions of temperature, airflow and pressure in the blade chamber were calculated based on which the typical mechanical weaknesses inside the blade were obtained based on the model. The results can provide theoretical guidance for blade design from the perspective of lightning protection.

II. MODELING OF INVASION OF LIGHTNING INDUCED ARC BY COUPLING THERMAL, ELECTROMAGNETIC AND AIRFLOW FIELDS

Due to the random properties of lightning, it is difficult to reproduce the process of invasion of lightning induced arc into the blade. Thus, a MHD model was adopted to

This work was supported in part by the National Natural Science Foundation of China (No. 51737005, 52127812, 51929701).

characterize the electromagnetic, thermal and airflow processes of the invasion arc.

The geometric models of the blades used in this paper are illustrated in Fig. 2. The cross section where the arc was hit in was chosen as the geometry model. The down conductor set in the blade chamber is used to lead the lightning current and it's usually installed along the blade web or the internal surface of main beam. Model 1 and model 2 represent the cross sections which are 2 m far away from the blade tip based on the typical down-conductor setup, namely, along blade web and along the internal surface of blade main beam. The red lines in the models represent the current-leading wires and it is assumed that the plasma generated by the impulse current distributes along the current-leading wire and the area vertically versus the wire, shown as the red-shadow areas. Considering that the blade webs have blocking effect on the multiphysics' distribution generated by the impulse current, the blue areas shown in the blade calculation models are selected to be the calculation domains.

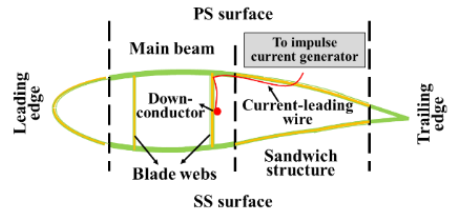

(a) Cross section of blade model 1

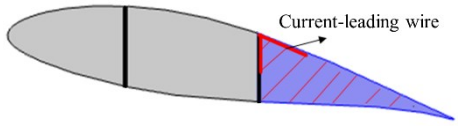

(b) Calculation domain of model 1

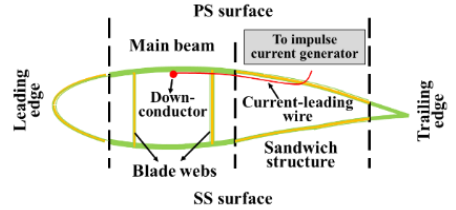

(c) Cross section of blade model 2

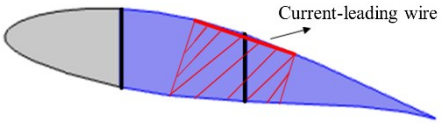

(d) Calculation domain of model 2

Fig. 2 Geometry models adopted in the simulation

In view of the three-dimensional asymmetric structure of the blade, some simplification methods are used to facilitate the calculation of the model. And given the typical development of lightning-induced arcs, we proposed the following assumptions for calculation.

a) It is assumed the current density to be the maximum at the current-leading wire, set as $\boldsymbol{J}_{max}$, and that $\boldsymbol{J}$ decreases linearly downward, set as 0 at the SS of the blade.

b) The direction of the current density $\boldsymbol{J}$ of the arc active region is considered to be parallel to the current-leading wire.

c) The arc development path laid along the inner surface of the blade is considered to be line segment l_{arc}. Particularly, the arc path is considered as a broken line in model 1. Each segment is solved separately and the results are added together while calculating this case.The arc development path laid along the inner surface of the blade is considered to be line segment l_{arc}. Particularly, the arc path is considered as a broken line in model 1. Each segment is solved separately and the results are added together while calculating this case.

Based on the assumptions above, the current density can be obtained by (1) and (2).

$$\int_0^{L_{ss}} J(r_1)dl = I \tag{1}$$

$$J(r) = J_{\max} - ar_1 \tag{2}$$

where r_1 refers to the vertical distance from any point in the calculation domain to l_{arc}, a is a linear attenuation rate, L_{ss} is the distance between the SS of the blade to the line segment l_{arc}, and I is the injection current, the value of which is obtained by (3).

$$I(t) = \begin{cases} I_{peak}\dfrac{t}{t_m} & t < t_m \\ I_{peak}\exp[-\alpha(t-t_m)] & t > t_m \end{cases} \tag{3}$$

where I_{peak} is the peak value of impulse current, being 30 kA, 90 kA, and 150 kA in this paper, t_m is the peak time of impulse current, being 25 μs according to experiment data, α refers to attenuation constant, being 0.003 in this paper.

After the current density is obtained, the distribution of magnetic induction $\boldsymbol{B}$ can be obtained according to Biot-Savart's law shown as (4), and the electric field strength $\boldsymbol{E}$ is obtained according to Ohm's law as (5).

$$\mathbf{B} = \int \frac{\mu_0 I(t)}{4\pi}\cdot\frac{d\mathbf{l}\times\mathbf{e}_{r_2}}{r_2^2} + \int \frac{\mu_0 I'(t)}{4\pi}\cdot\frac{d\mathbf{l}\times\mathbf{e}_{r_2}}{cr_2} \tag{4}$$

$$\mathbf{J} = \sigma\mathbf{E} \tag{5}$$

where, μ_0 is the magnetic permeability, d$\boldsymbol{l}$ is the line integral element, $\boldsymbol{e}_{r2}$ is the unit direction vector between the current element and the point to be calculated, r_2 is the distance between the point to be determined and the direction vector, σ is the conductivity, $I'(t)$ is derivative of the current value versus time, c is the speed of light.

Equations (6) to (8) are fluid dynamic equations composed of continuity equations, momentum conservation, and energy conservation equations. The current density $\boldsymbol{J}$, the magnetic induction $\boldsymbol{B}$ and the electric field strength $\boldsymbol{E}$ obtained above will be brought into (6) to (8), from which the internal temperature, airflow and pressure distribution of the blade under the lightning arc can be calculated.

This paper is a peer reviewed, accepted author manuscript of the following research paper: Yu, W., Li, Q., Guo, Z., Ren, H., & Siew, W. H. (2022). Numerical study on explosion characteristics of wind turbine blade under lightning induced arc. In 2022 IEEE International Symposium on Electromagnetic Compatibility & Signal/Power Integrity (EMCSI) IEEE. https://doi.org/10.1109/EMCSI39492.2022.9889347

$$\frac{\partial \rho}{\partial t}+\nabla\cdot(\rho\mathbf{u})=0 \tag{6}$$

$$\frac{\partial \rho\mathbf{u}}{\partial t}+\rho(\nabla\cdot\mathbf{u})\mathbf{u}=-\nabla p+\nabla\cdot[\mu(\nabla\mathbf{u}+(\nabla\mathbf{u})^{\mathrm{T}})-\frac{2}{3}\mu(\nabla\cdot\mathbf{u})\mathbf{A}]+\rho\mathbf{g}+\mathbf{J}\times\mathbf{B} \tag{7}$$

$$\frac{\partial(\rho C_p T)}{\partial t}+\nabla\cdot(\rho C_p T\mathbf{u})=\nabla\cdot(k\nabla T)+\sigma E^2+q_{rad}+q_{\eta} \tag{8}$$

where ρ is the fluid density, p is the pressure, T is the temperature, u is the fluid velocity, R_s is the gas constant, μ is the dynamic viscosity, g is the gravity acceleration, C_p is the fluid constant pressure heat capacity, k is the thermal conductivity, q_{rad} is radiant heat, being 0 in this paper, q_n= 0 refers to viscous heat.

The models were computed by the finite element method in Comsol Multiphysics. The computational domain was divided into meshes with a minimum mesh length of 0.65 mm and a maximum of 14.4 mm. In addition, the transient calculation time step was set to 10 μs.

To prove the validity of the model, the pressure range at the trailing edge of the blade was obtained by applying lightning parameter with time properties of 1.2/50μs, 10/100μs, 18/200μs and 25/250μs and amplitude of 30kA, shown in table 1.

TABLE I. MAXIMUM VALUE OF PRESSURE AT THE TRAILING EDGE UNDER THE CURRENT WITH PEAK VALUE OF 30KA

Blade type	Model 1	Model 2
Air pressure at the trailing edge (×10^{4}Pa)	15~55	2.5~10

It's pointed out that the epoxy resin is treated as adhesive to stick the upper and the nether skins at the trailing edge of blade. Therefore, the mechanical strength of the trailing edge is determined by the ability of the adhesive, known also as peel strength. The typical peel strength of epoxy resin ranges from 79 to 315 N/ 25mm, representing that the maximum pressure can be suffered by the epoxy resin is 15 to 63 kilopascal after conversion, close to the data shown in Table. 1.

III. SIMULATION RESULTS

The distribution of current and magnetic induction can further lead to heat transfer, airflow, and even impact pressure in the blades. The comparisons of temperature, airflow and pressure distributions between model 1 and model 2 are shown from Fig. 3 to Fig. 8(when the peak value of impulse current is 90kA). The impulse current first generates high temperature near the current-leading wire (shown in Fig. 3, Fig. 6), then the high temperature area gradually diffuses into the whole blade chamber, which causes the air flowing rapidly in the chamber (the speed distributions of airflow are shown in Fig. 4, Fig. 7). Fast flowing air in the blade chamber impacts on the blade inner surface (pressure distributions in the blade are shown in Fig. 5, Fig. 8), eventually causing structural damage to the blade. From the pressure distribution inside the two models, it can be found that the boundary between the upper inner surface of the blade and the blade web near the trailing edge will be subjected to a large pressure, and then the high-pressure area will spread further. The narrow areas inside the blade chamber such as nether inner surface of the blade and the bonding point of trailing edge are subject to high pressure threats.

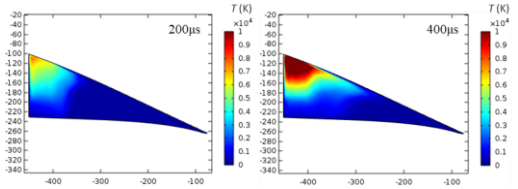

Fig. 3 Temperature distribution in Model 1 (K)

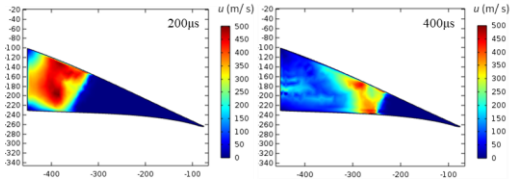

Fig. 4 Velocity distribution of airflow in Model 1 (m/s)

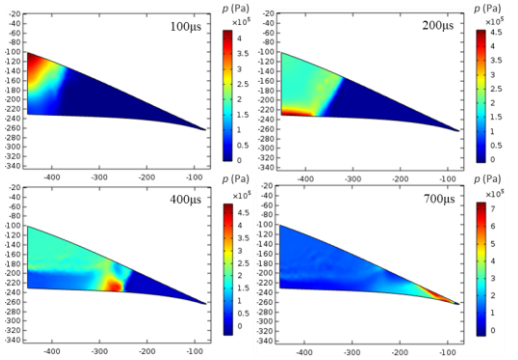

Fig. 5 Pressure distribution in Model 1 (Pa)

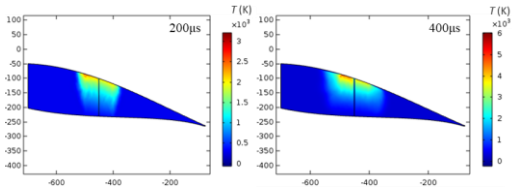

Fig. 6 Temperature distribution in Model 2 (K)

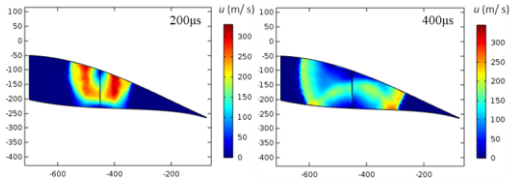

Fig. 7 Velocity distribution of airflow in Model 2 (m/s)

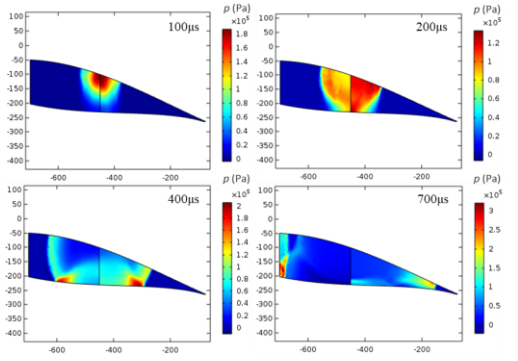

Fig. 8 Pressure distribution in Model 2 (Pa)

This paper is a peer reviewed, accepted author manuscript of the following research paper: Yu, W., Li, Q., Guo, Z., Ren, H., & Siew, W. H. (2022). Numerical study on explosion characteristics of wind turbine blade under lightning induced arc. In 2022 IEEE International Symposium on Electromagnetic Compatibility & Signal/Power Integrity (EMCSI) IEEE. https://doi.org/10.1109/EMCSI39492.2022.9889347

When the down conductor is set along the blade web (model 1), it can be found that the energy generated by the impulse current can be blocked between the trailing web and the trailing edge of blade, thus the heat and pressure get higher and change faster in this area than those in model 2. The bonding places inside the blade are usually considered as the mechanical weaknesses of the blade, such as the bonding between the trailing web and the upper inner surface (marked as bonding 1 in this paper), the bonding between the trailing edge and the nether inner surface (bonding 2) and the bonding at the trailing edge (bonding 3). The pressure variations at the three weak locations are depicted in Figure 9, showing that the peak pressures at the weak locations in Model 1 are 2.3, 2.7 and 5.5 times higher than those in Model 2, respectively.

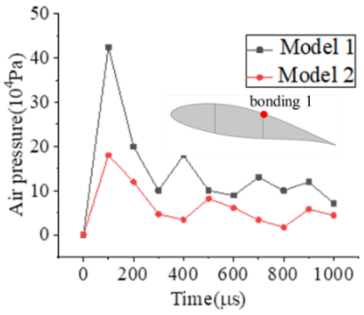

(a) The pressure at bonding 1

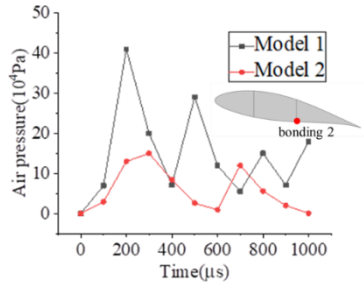

(b) The pressure at bonding 2

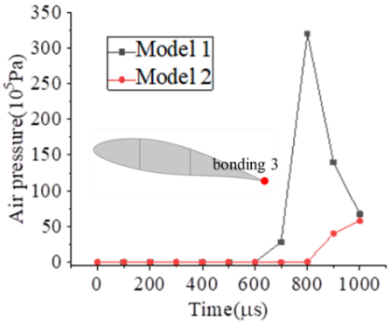

(c) The pressure at bonding 3

Fig. 9 Pressure at bonding places in Model 1 and Model 2 (Pa).

IV. Conclusion

In order to calculate the multiphysics distributions in the blade chamber, the MHD model of impulse arc in the blade considering the arc paths was established in this paper. The distributions of temperature, airflow and pressure in the blade chamber were calculated.

It's found that the narrow spaces referring to the bonding places are subjected to higher pressure, such as the boning of webs and inner surface of the blade, and the boning at the trailing edge. When the down conductor is set between the trailing web and the trailing edge, the pressure suffered by the trailing edge is much higher compared with that when fixing the down-conductor between the two blade webs. Thus, the improvement of the structure design in the blade should be conducted accordingly.

References

[1] A. C. Garolera, S. F. Madsen, M. Nissim, J. D. Myers, and J. Holboell, "Lightning Damage to Wind Turbine Blades From Wind Farms in the U.S.," *IEEE Trans. Power Deliv.*, vol. 31, no. 3, pp. 1043–1049, Jun. 2016, doi: 10.1109/TPWRD.2014.2370682.

[2] "IEC 61400-24: 2010 Wind turbine generator systems-Part 24: Lightning protection," IEC, 2010.

[3] B. M. Radičević, M. S. Savić, S. F. Madsen, and I. Badea, "Impact of wind turbine blade rotation on the lightning strike incidence – A theoretical and experimental study using a reduced-size model," *Energy*, vol. 45, no. 1, pp. 644–654, Sep. 2012, doi: 10.1016/j.energy.2012.07.032.

[4] S. Yokoyama, "Lightning protection of wind turbine blades," *Electr. Power Syst. Res.*, vol. 94, pp. 3–9, Jan. 2013, doi: 10.1016/j.epsr.2012.07.017.

[5] Q. Li *et al.*, "The lightning striking probability for offshore wind turbine blade with salt fog contamination," *J. Appl. Phys.*, vol. 122, no. 7, p. 073301, Aug. 2017, doi: 10.1063/1.4999311.

[6] W. Yu, Q. Li, J. Zhao, H. Li, and W. H. Siew, "Thundercloud-Induced Spatial Ion Flow in the Neighborhood of Rotating Wind Turbine and Impact Mechanism on Corona Inception," *IEEE Trans. Plasma Sci.*, vol. 49, no. 9, pp. 2925–2935, Sep. 2021, doi: 10.1109/TPS.2021.3102376.

[7] Y. Wang and O. I. Zhupanska, "Lightning strike thermal damage model for glass fiber reinforced polymer matrix composites and its application to wind turbine blades," *Compos. Struct.*, vol. 132, pp. 1182–1191, Nov. 2015, doi: 10.1016/j.compstruct.2015.07.027.

[8] J. Yan *et al.*, "A Comparative Study on Damage Mechanism of Sandwich Structures with Different Core Materials under Lightning Strikes," *Energies*, vol. 10, no. 10, p. 1594, Oct. 2017, doi: 10.3390/en10101594.

[9] T. Ogasawara, Y. Hirano, and A. Yoshimura, "Coupled thermal–electrical analysis for carbon fiber/epoxy composites exposed to simulated lightning current," *Compos. Part Appl. Sci. Manuf.*, vol. 41, no. 8, pp. 973–981, Aug. 2010, doi: 10.1016/j.compositesa.2010.04.001.

[10] Y. Goda, S. Tanaka and T. Ohtaka, "Arc tests of wind turbine blades simulating high energy lightning strikes," *in 2008 International Conference on Lightning Protection (ICLP)*, 2008, pp. 1–4.

This paper is a peer reviewed, accepted author manuscript of the following research paper: Yu, W., Li, Q., Guo, Z., Ren, H., & Siew, W. H. (2022). Numerical study on explosion characteristics of wind turbine blade under lightning induced arc. In 2022 IEEE International Symposium on Electromagnetic Compatibility & Signal/Power Integrity (EMCSI) IEEE. https://doi.org/10.1109/EMCSI39492.2022.9889347